

The Impact of Surface Hydrology on the Simulation of Tropical Intraseasonal Oscillation in NCAR (CCM2) Atmospheric GCM

K. RAJENDRAN¹, Ravi S. NANJUNDIAH and J. SRINIVASAN

Centre for Atmospheric & Oceanic Sciences, Indian Institute of Science, Bangalore, India

(Manuscript received 6 December 2000, in revised form 13 August 2002)

Abstract

The impact of surface hydrological processes in the simulation of tropical climate by the Community Climate Model Version 2 (CCM2) has been studied. Two ten year climate simulations have been analysed to study the effect of surface hydrology feedback. In one of the simulations the surface moisture was determined interactively (VAR_HYD), while in the other simulation the surface moisture was fixed to annual climatological values (FIX_HYD). The simulated values of soil moisture in the VAR_HYD simulation are higher than the annual climatological values, both during northern summer and winter seasons. The impact of surface hydrology on precipitation was larger during northern summer than during the northern winter season. The impact of surface hydrology specification was found to be not entirely local in the model. It appears to have a remote impact on the other parts of the tropics. The precipitation increased over the Indian region, and off-equatorial West Pacific in the interactive hydrology simulation (vis-a-vis FIX_HYD) and reduced over the equatorial West Pacific regions. The simulation of precipitation also improves over the East Pacific region with the incorporation of interactive hydrology. The differences in precipitation between the VAR_HYD and the FIX_HYD simulations are associated with differences in vertical moist static stability and 500 hPa vertical velocity.

From harmonic analysis of OLR it was found that the power and frequency in the intraseasonal scales is simulated more realistically with the incorporation of interactive surface hydrology. The interactive hydrology was found to be necessary for the simulation of meridional propagations of convective zones over the Indian region (on intraseasonal time-scales). The meridional migration is not observed in the simulation with fixed surface hydrology, and is on account of non-monotonic variation of vertically integrated moist static energy. The specification of continental surface hydrological processes did not however have a significant impact on the simulation of the equatorially trapped waves, such as the Madden-Julian Oscillation (MJO), though the propagations are discontinuous in the FIX_HYD simulation.

1. Introduction

Surface hydrological processes play a key role in modulating atmospheric convection. The amount of moisture available in continental regions for evaporation is limited by the soil moisture (in contrast to oceans where it is al-

most unlimited for all practical purposes), and plays a crucial role in determining surface temperature and locally available moisture for sustaining moist convection. Most studies involving surface hydrological effects focus on the issue of interannual variability and the interaction between surface hydrological effects and interannual variation of SST. Yang and Lau (1998) suggest that surface hydrological effects occur in conjunction with warm SST events. They find that during warm SST events there is higher snow cover, and more soil moisture over the Eurasian region. This leads to the

Corresponding author: Ravi S Nanjundiah, Centre for Atmospheric & Oceanic Sciences, Indian Institute of Science, Bangalore-560 012, India.
E-mail: ravi@caos.iisc.ernet.in

¹ Current Affiliation: Meteorological Research Institute, Tsukuba, Ibaraki 305-0052, Japan
© 2002, Meteorological Society of Japan

weakening of the monsoon. Shen et al. (1998) have studied the impact of land-surface processes on the interannual variability of the large-scale Asian monsoon with the CCSR/NIES AGCM. They conclude that the ENSO related changes to predominate over the land-surface processes. Goswami (1998) suggests that internal feedbacks, such as surface hydrological effects, give rise to a Quasi-Biennial Oscillation (QBO) in the GFDL model's simulation.

Bras (1999) has suggested that over continental regions, surface-hydrological feedback is perhaps the most important factor in determining the mean seasonal precipitation. His results indicate (Fig. 9, Bras 1999) clearly that when soil moisture specified from observations is used, a realistic mean seasonal pattern of precipitation is obtained over the continental USA. He has also shown that if soil moisture is specified from climatology, there are large errors in the simulation of precipitation in the mid-western region of the USA.

The impact of surface hydrological specification on the seasonal mean simulation of the tropical climate, and its intraseasonal variation has, however, not been extensively studied with GCMs. Most such studies have been conducted with simple phenomenological models. These studies (Webster 1983; Gadgil and Srinivasan 1990; Nanjundiah et al. 1992) showed that specification of surface hydrology has a strong impact on the intraseasonal variations. Webster (1983) suggested that the poleward gradient of sensible heat flux was the cause of poleward propagations of rainbands over the Indian monsoon region. Nanjundiah et al. (1992) and Gadgil and Srinivasan (1990) showed that it was the poleward gradient of vertical atmospheric instability, rather than the poleward gradient of sensible heat flux, that was responsible for the occurrence of poleward propagations of rainfall bands.

In this paper we study the impact of surface hydrology specification on the simulation of tropical climate on seasonal and intraseasonal scales with the NCAR CCM2. Simulations with two versions of the NCAR CCM2 model have been performed. One with hydrology fixed to annual mean climatological values (referred to as FIX_HYD) and the other with an interactive surface hydrology (referred to as VAR_HYD).

While more sophisticated atmosphere-land surface interchange models, such as BATS and SiB are available, we have used the simple bucket scheme of Manabe et al. (1965). The work of Robock et al. (1998) has shown that more complicated surface hydrological models (including multi-layer models) do not imply better simulations.

The ability of a model to reproduce the intraseasonal variations is related to its simulation of the seasonal mean climate (Slingo et al. 1996), and therefore we first study the mean simulated climate over the tropics, followed by a discussion of intraseasonal variations. In this paper, section 2 describes the model, data and the methodology, including the design of the experiments. In section 3, we discuss the simulation of seasonal mean climate over the tropics. The effect of surface hydrology specification on the seasonal cycle is presented in section 4. The simulation of intraseasonal oscillations by the two versions of the model is given in sections 5 and 6, respectively. In section 7, we summarize the results.

2. The model, data and methodology

2.1 *The model*

A scalable parallel message-passing implementation of the National Centre for Atmospheric Research Community Climate Model, Version 2 (NCAR CCM2), developed by Argonne and Oak Ridge National Laboratories (Drake et al. 1995) has been used in this study. This model (CCM2) has been widely used for various climate studies (Hack et al. 1994; Kiehl et al. 1994; Lieberman et al. 1994; Zhang et al. 1994; Hahmann et al. 1995 and others). The detailed documentation of the model can be found in Hack et al. (1993).

Since the difference between the two simulations is the prescription of surface hydrology over the continental regions, we include a brief discussion of the simple bucket hydrology used in the VAR_HYD simulation. In the FIX_HYD simulation, the surface wetness is specified to its annual mean climatological value.

The surface hydrology parameterization scheme (based on Manabe et al. 1965) used in the VAR_HYD simulation is the simple, bucket model of Holloway and Manabe (1971). In this scheme, the land surface at each grid point is represented by a single layer that fills with

precipitation, empties by evaporation and over-flow producing runoff. In this single-layer scheme, the wetness factor (D_w) is determined from a budget of evaporation, precipitation and runoff. Over ocean, and over snow cover, the wetness factor (D_w) is set to 1, i.e., evaporation is assumed to be from a saturated surface.

Over land, the soil moisture is forecast by adding rainfall and snow melt to the existing soil moisture and subtracting evaporation and runoff. The precipitation from convection is assumed to be rain if either the surface temperature or the temperature in either of the first two atmospheric layers above the surface is greater than or equal to 273.16 K. Otherwise, the precipitation is assumed to be snow.

In the simplified bucket model, the soil moisture value, 'W' is modified after each time step using the computed evaporation, and precipitation during that time step:

$$\frac{\partial W}{\partial t} = P - E + S_m,$$

where, P is the total rainfall rate, E is the evaporation rate and S_m is the rate of snow melt.

When the soil moisture reaches the soil field capacity (W_{FC}), the maximum amount of water that can be stored in the soil, the excess above the field capacity is assumed to form runoff (r_f). If $W > W_{FC}$, the runoff over a given time step is given by $r_f = W - W_{FC}$ and W is then reset to W_{FC} . The filed capacity is taken to be $W_{FC} = 15$ cm. This runoff does not affect any other neighboring grid-points.

The new wetness value is computed as,

$$W_{new} = W_{old} + \frac{\partial W}{\partial t} \Delta t.$$

The wetness factor, D_w , which is used in the computation of evaporation rate (E) is determined from the soil moisture following the 'tilted bucket' scheme as,

$$D_w = \begin{cases} 1 & \text{if } W \geq W_C \\ \exp \left[\frac{\left(1 - \frac{W}{W_{FC}}\right)^2}{\left(1 - \frac{W}{W_{FC}}\right)^2 - 1} \right]^{1.25} & \text{if } W < W_C, \end{cases}$$

where, W_C is a critical fraction of the soil field capacity given as $W_C = 0.75 W_{FC}$, at which the

evaporation rate becomes equal to its potential value.

2.2 Data

The sea surface temperature (SST), and sea ice distributions, are specified from the climatological data and updated in the middle of each month. The SST data set used in the model is from Shea et al. (1990) and interpolated for each model time step between the mid-month values. Thus, the model is basically forced by the seasonal change of SST, and the daily change of the solar declination angle with a fixed solar insolation of 1370 W m^{-2} at the top of the model atmosphere. The model integration is started from the initial conditions corresponding to 1st September 1987 (an analysis data set provided by NCAR), and is integrated for 10 model years. The first three months of integrations are not considered for analysis, to remove the model spin-up effects. Since the two sets of 10 year model integrations have been performed with climatological SST, each of the climate simulations can also considered to be equivalent to a set of 10 ensembles of one year duration (with identical external and boundary forcing, but differing initial conditions).

For comparison with model simulated precipitation, observed monthly precipitation data sets, based on the CPC (Climate Prediction Center) merged analysis of precipitation (Xie and Arkin 1997, henceforth referred to as 'Xie-Arkin') were used. In addition, the GPCP daily rainfall estimate (Huffman et al. 2000), and MSU daily rainfall (Spencer 1993), has also been used for comparison on the intraseasonal scales. Over the Indian region, we have analysed the rainfall data at 366 meteorological observatories, supplied by the India Meteorological Department (IMD), which is henceforth referred to as IMD data. The observed interpolated (Liebmann and Smith 1996) outgoing longwave radiation (OLR), obtained from the Advanced Very High Resolution Radiometer (AVHRR) on National Oceanic and Atmospheric Administration (NOAA) polar orbiting satellite, as daily data from 1979 to 1997 on a 2.5° latitude-longitude grid (Gruber and Winston 1978; Gruber and Krueger 1984), has also been used. For validation of circulation fields, and for the computation of moist static energy,

NCEP/NCAR daily and monthly reanalysis products (Kalnay et al. 1996) have been used.

For spectral analysis, global datasets on daily scales for long periods (about 10 years) are required. But such datasets are not available for precipitation, hence we have used OLR as proxy for rainfall. For consistency we have compared model-generated OLR with observed OLR.

2.3 Methodology

Simulated seasonal, and intraseasonal variation, have been studied using harmonic analysis in both spatial and temporal dimensions. The ability of the model to simulate the intraseasonal variation has been examined by identifying dominant periodicities through power spectrum analysis. The simulation of the MJO propagation characteristics has been assessed using OLR and 200 hPa circulation fields after applying 20–70 day Lanczos band-pass filter (Duchon 1979), and their spectral characteristics using the space-time spectral technique (Hayashi 1977, 1982). The time-lagged correlation analysis has been used to identify the simulation of meridional propagation of convective zones. We also have attempted to understand the association between surface moist static enthalpy, and the simulation of propagations in the two versions of the model.

3. Simulation of seasonal mean climate over the Tropics

The model simulated 10 year mean tropical average OLR (0–360°; 30°S–30°N) for the summer (JJA) and winter (DJF) months, and the annual mean, have been compared with the long term mean (1980–1995) observed OLR in Table 1. The two versions of the model simulate lower OLR during winter than in summer. It is seen that in both seasons the simulated OLR is higher than the observed OLR. The seasonal,

and the annual average OLR values, are comparable between the two simulations. The difference between the observed and simulated values are of the order of 10 W m^{-2} in both the simulations.

The total OLR consists of OLR from clear sky and from clouds, and hence depends on the fraction of area covered by clouds. Fraction of cloud cover in the model is estimated through a cloud scheme (Kiehl et al. 1994, a modified version of Slingo 1987) using convective precipitation rate, specific humidity and temperature in the model. The comparison of model simulated total cloud cover with the International Satellite Cloud Climatology Project (ISCCP) data (Rossow and Schiffer 1991) averaged for 1983–1991 show that the model underestimates the percentage of total cloud cover over the tropics in both winter and summer seasons. The total cloud cover from both versions of the model are lower than the estimates based on ISCCP C2 data (Table 2). The difference in the observed, and simulated OLR values, can be partly due to the lower fraction of cloud cover over the tropics in the model.

The observed and VAR_HYD simulated winter mean (10 year December-January-February mean) OLR and the difference between VAR_HYD and FIX_HYD winter mean OLR, are shown in Fig. 1. In the seasonal mean patterns, the regions with OLR values less than 240 W m^{-2} are shaded. It is well established that in tropics, the OLR flux less than 240 W m^{-2} indicates the presence of deep clouds (e.g., Waliser et al. 1993). In northern winter, the observed OLR in the tropics is less than 220 W m^{-2} over a very large region extending from around 60°E to the dateline and roughly from 5°N to 5°S (Fig. 1a). The regions with simulated OLR less than 220 W m^{-2} is much smaller, and restricted to Indonesia and Brazil (Fig. 1b). The model underestimates the con-

Table 1. Seasonal and annual mean OLR (W m^{-2}) averaged over the tropics (0–360°; 30°S–30°N).

	JJA	DJF	Annual
Observation	252.1	248.3	250.6
VAR_HYD	264.4	259.9	262.4
FIX_HYD	264.1	258.4	261.4

Table 2. Seasonal and annual mean total cloud cover (%) averaged over the tropics (0–360°; 30°S–30°N).

	JJA	DJF	Annual
ISCCP C2	58.1	57.9	58.0
VAR_HYD	47.3	49.8	48.7
FIX_HYD	48.4	50.4	49.4

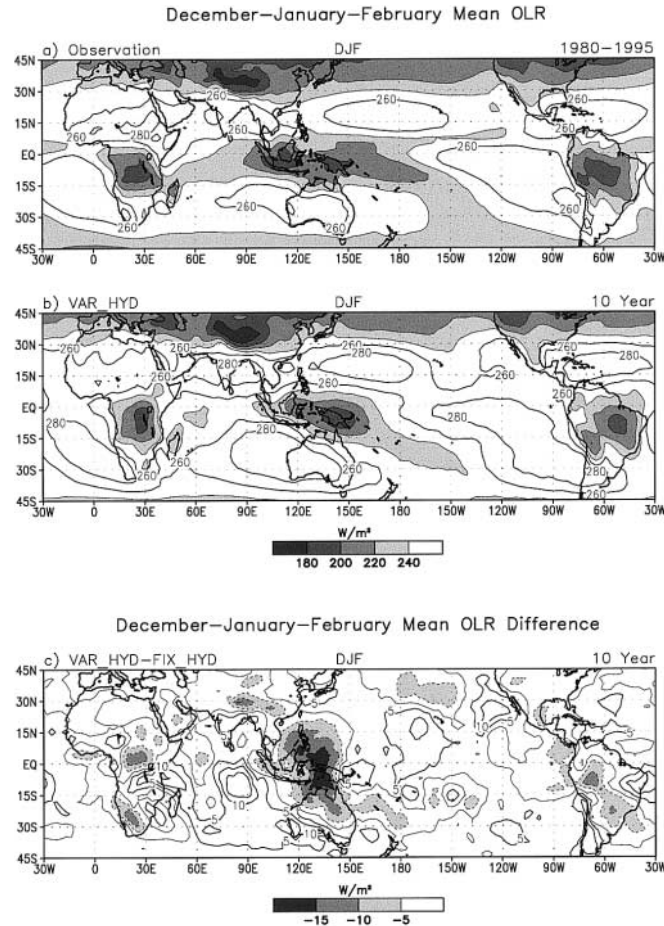


Fig. 1. Mean OLR for Northern Hemispheric winter (DJF) season for: (a) observation; (b) VAR_HYD simulation; and, (c) the difference between the winter mean VAR_HYD and FIX_HYD OLR simulations.

vective activity over the tropical southern Indian Ocean. But the location and intensity of convective activity over the southern African, and South American regions are simulated realistically by both versions of the model.

During northern winter, the regions of deep convection is centered over southern Africa, a broad region of convection extending from 60°E, to dateline over the north Australia-Indonesian region, and over northern parts of South America (Fig. 1a). The simulation gives a reasonable OLR distribution over the regions north of 35°N, though these are not related to deep convection. The model is unable to simulate low OLR values over the oceanic regions of South Indian Ocean and South Pacific Ocean. During winter, the difference between the sim-

ulations are much smaller over most of the tropics except over the southern Indian Ocean and the northern parts of Australia (Fig. 1c). The impact of changes in surface hydrology is most pronounced over the maritime continents of the West Pacific and over the seasonal convective centres of South America, and parts of Africa.

The observed, and VAR_HYD simulated northern summer mean (10 year June-July-August mean) OLR, and the difference between VAR_HYD and FIX_HYD summer mean OLR, are shown in Fig. 2. In boreal summer, the observed organized deep convection is mainly confined to the Asian monsoon region and over the western Pacific warm pool region with an eastward extension to the Inter-Tropical Con-

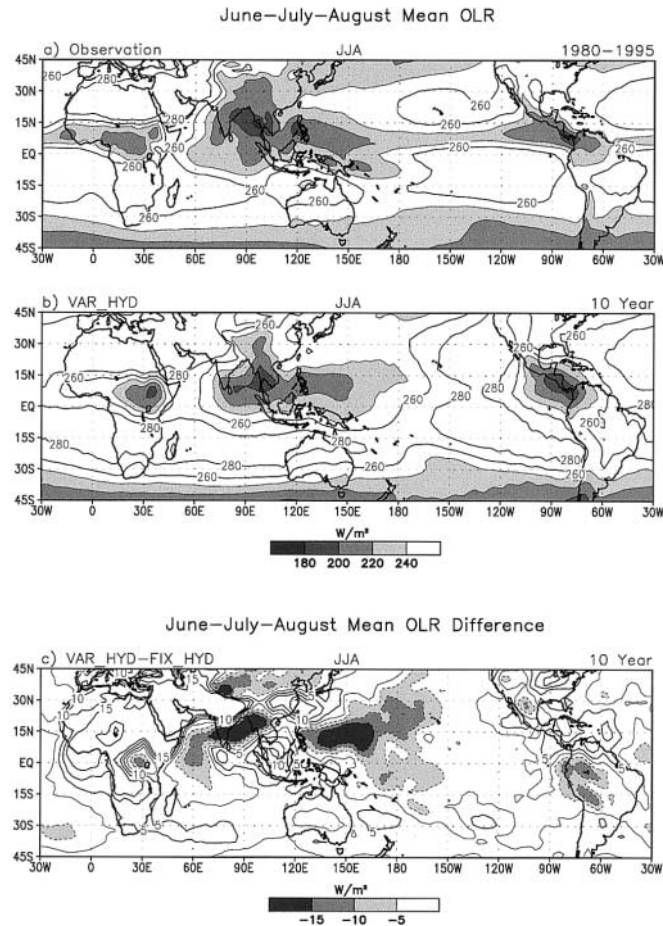


Fig. 2. Mean OLR for Northern Hemispheric summer (JJA) season for: (a) observation; (b) VAR_HYD simulation; and, (c) the difference between the summer mean VAR_HYD and FIX_HYD OLR simulations.

vergence Zone (ITCZ) in the eastern Pacific and central America (Fig. 2a). Deep convection over the northern parts of Africa and South America is simulated reasonably well by both the versions of the model (Fig. 2b). Over the Indian subcontinent, the observation shows large regions with low OLR (i.e., less than 220 W m^{-2}) associated with the Indian summer monsoon, but the model simulation does not capture this feature realistically. The OLR values are greater than 260 W m^{-2} in the southern Indian Ocean, the north eastern and south eastern Pacific, and north and south Atlantic regions indicating cloud free regions. In the simulation, the ITCZ over the Pacific east of the dateline is absent. The simulated OLR over the Northern Hemispheric land mass is larger than the observation. This could be due to the persistent

warm surface temperature bias in the model especially over the Northern Hemispheric land regions as shown by Kiehl et al. (1994).

Figure 2c shows the difference between summer mean OLR from VAR_HYD and FIX_HYD simulations. In summer, the regions with maximum difference between the two simulations (Fig. 2c) is located over the Indian region, West Pacific and over northern parts of Africa and South America. This shows that in the variable hydrology case, the strength of deep convection increases over the off-equatorial Asia-West Pacific, and South American regions, and decreases over the north African and near equatorial West Pacific regions.

We note that the impact of surface hydrology specification is more over the seasonal convective centres (Asia-Pacific region, northern parts

of Africa and South America in summer; maritime continents of West Pacific and southern parts of Africa and South America in winter) of the tropics, with deep convection being stronger in the variable hydrology case.

3.1 Vertical stability and precipitation

Although the variable hydrology specification changes the surface hydrology only over the continental regions, the differences (Figs. 1c & 2c) in the simulated OLR patterns show that the impact of the surface hydrology is not entirely local. This fact is established by the large increase in the simulated convection over the warm oceanic regions of the Bay of Bengal, and off-equatorial West Pacific and decrease over the southern Indian ocean and near equatorial West Pacific in the variable hydrology case during summer. This is on account of the existence of teleconnections between convective activity over the Indian and West Pacific regions (Joseph and Srinivasan 1999).

Comparing the Vertical Moist Static Stability (VMS, defined as the difference in the layer-averaged moist static enthalpy between the upper and the lower troposphere, lower layer being 1000 hPa–400 hPa, upper layer being 400 hPa–50 hPa), we note that the difference in VMS (Fig. 3c) between the two simulations has the same pattern as the difference in organized large-scale convection (Fig. 3a). This can be understood with the simple model developed by Neelin and Held (1987) based on moist static energy budget. Nanjundiah (2000), Nanjundiah and Srinivasan (1999) and Zhang (1994) have used this simple model to demonstrate association between variations in VMS and precipitation.

We can write the relationship between VMS and precipitation in the following way (Zhang 1994):

$$\frac{\Delta P}{P} \approx -\frac{\Delta m}{m}. \quad (1)$$

Here m , is the vertical moist static stability (VMS) and P , the precipitation. This implies that increase in rainfall, P , is associated with decrease in VMS, m .

We note that the decrease in VMS over the Indian Region and increase in VMS over the near-equatorial West Pacific Region in the VAR_HYD simulation vis-a-vis FIX_HYD is

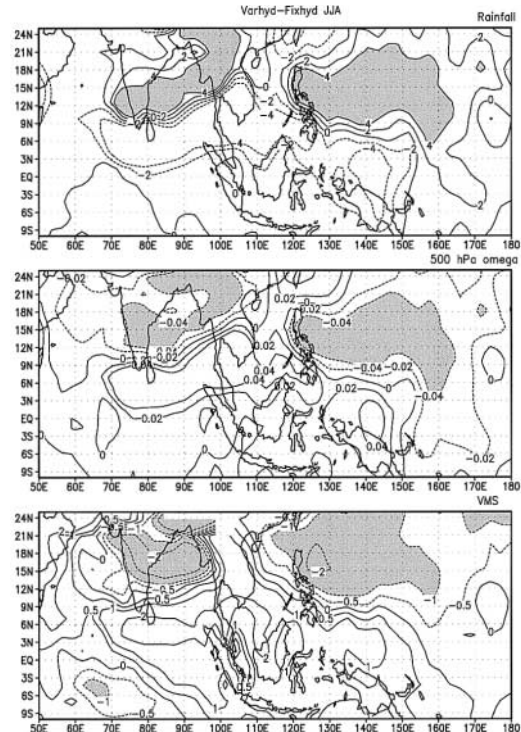


Fig. 3. The difference between the summer (JJA) mean VAR_HYD and FIX_HYD simulated: (a) precipitation (mm day^{-1}); (b) 500 hPa vertical velocity (cm sec^{-1}); and, (c) VMS (kJ kg^{-1}).

consistent with the changes in precipitation over these regions (i.e., increase in rainfall over the Indian region and decrease in rainfall over the West Pacific region) during the JJA season. Similar differences are also seen over South America and equatorial Africa. As discussed earlier, we note the non-local effect of surface hydrological changes between the two simulations especially over oceanic regions, such as the West Pacific. The change in VMS can be understood in terms of changes in the circulation patterns. Figure 3b shows the 500 hPa JJA vertical velocity. We note that the regions of increase (decrease) in VMS are associated with regions of weaker (stronger) ascent in the variable hydrology simulation vis-a-vis the fixed hydrology simulation. The weaker ascent (or stronger descent) causes the atmosphere to be more stable thus inhibiting organized convective activity. In the VAR_HYD simulation the moist ground increases the moisture in the

air-column above (due to enhanced evaporation) reducing its static stability. Associated with this reduced stability is the enhanced convective activity over the Indian Monsoon region. This in turn changes the circulation pattern causing reduced ascent (and thus increasing the stability and reducing the associated precipitation), over the equatorial West Pacific region. It is interesting to note that a similar pattern of increased ascent over the Indian region and reduced ascent over the West Pacific region can be seen in the 500 hPa vertical wind anomaly pattern for the year 1961, which had experienced the highest rainfall over the Indian monsoon region during the 20th century. It is also noteworthy that an increase in rainfall in the VAR_HYD simulation over the Indian monsoon region is associated with an increase in precipitation over the off-equatorial West Pacific. Similar changes have

also been observed during certain years (e.g., 1988).

The remote impact can also be understood through the differences in circulation. Figure 4a shows the 850 hPa wind patterns, and the differences between the VAR_HYD and FIX_HYD simulations. In Fig. 4b we show the 200 hPa winds. These two figures show that in VAR_HYD simulation the prominent features of summer monsoon circulation such as the low level westerlies, are more organized along the east African coast, stronger over the Indian peninsular region and penetrates deeper into the West Pacific compared to the FIX_HYD simulation. This in turn increases the ascent and convection over the Indian region, and off-equatorial West Pacific (as seen in Fig. 3). This enhanced circulation over northern India-West Pacific region is also evident in the upper level easterlies and associated divergence.

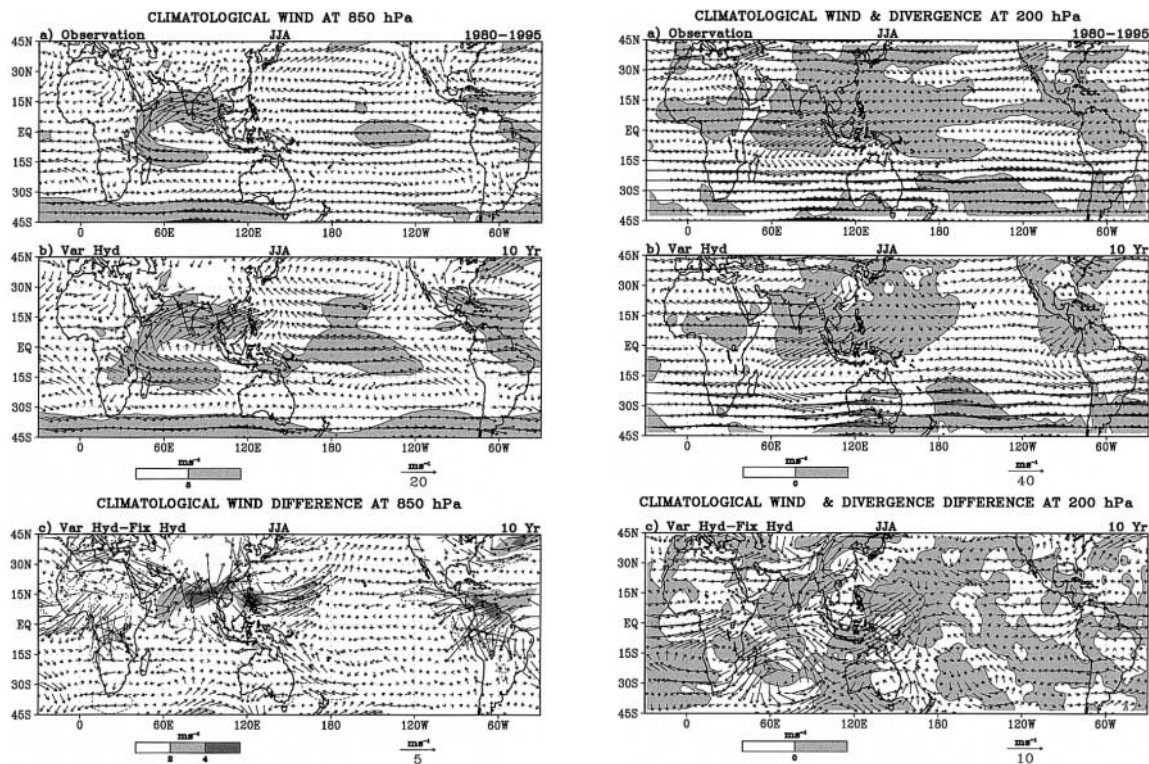


Fig. 4a. Climatological 850 hPa winds from (top) NCEP analysis, (middle) VAR_HYD and (bottom) difference between VAR_HYD and FIX_HYD for JJA season.

Fig. 4b. Climatological 200 hPa winds (arrows) and divergence (shaded) for (top) NCEP reanalysis, (middle) VAR_HYD and (bottom) difference between VAR_HYD and FIX_HYD simulations for JJA season.

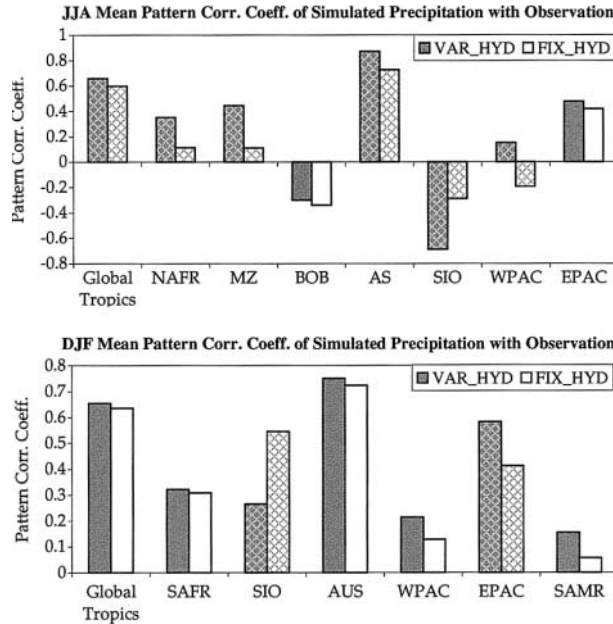


Fig. 5. Pattern correlation coefficient of June-July-August (top) and December-January-February (bottom) average precipitation with respect to observed Xie-Arkin precipitation for VAR_HYD and FIX_HYD simulations. PCCs for the regions where the difference in correlation between VAR_HYD and FIX_HYD simulations is significant at 90% level are hatched. The selected regions are: Global tropics (0–360°, 30°S–30°N); North Africa, NAFR (10°E–30°E, 0–12.5°N); Monsoon Zone, MZ (70°E–85°E, 15°N–27.5°N); Bay of Bengal, BOB (80°E–95°E, 7.5°N–17.5°N); Arabian Sea, AS (55°E–70°E, 7.5°N–17.5°N); South Indian Ocean, SIO (67.5°E–92.5°E, 12.5°S–0); West Pacific, WPAC (120°E–142.5°E, 5°N–17.5°N); East Pacific, EPAC (90°W–130°W, 0–15°N); South Africa, SAFR (15°E–35°E, 15°S–2.5°S); Australia, AUS (122.5°E–142.5°E, 25°S–15°S); and, South America, SAMR (45°W–67.5°W, 15°S–2.5°S).

3.2 Pattern correlation

To study the effect of changed surface hydrology on the simulation of mean precipitation pattern over the tropics, we have compared the Pattern Correlation Coefficient (PCC) with respect to observations from the two simulations over different regions of the tropics. The regions have been selected so that they represent the major convective centres during Northern Hemispheric summer and winter seasons. Figure 5 shows the PCC of summer and winter mean precipitation (with respect to Xie-Arkin precipitation) from VAR_HYD and FIX_HYD simulations for the selected regions. (The regions selected and their geographic locations are given in the figure caption.) For both seasons, the PCCs for the regions where the difference in correlation between VAR_HYD and FIX_HYD simulations is significant at 90% level are hatched. A student's *t*-test is applied

after a Fisher's *Z* transformation of the correlations to test the significance of the difference in correlation.

During summer, the simulations are correlated reasonably well with the observation over the whole tropics. The difference in correlations are significant at 90% level except for the Bay of Bengal (where the PCCs are negative) and East Pacific. Over North Africa, Monsoon Zone, Arabian Sea and East Pacific, the VAR_HYD simulation shows higher pattern correlation with observations than the FIX_HYD simulation. However, over the Bay of Bengal, the South Indian Ocean and West Pacific, both the simulations are poor and the change in the surface hydrology specification does not have any positive impact on the PCC. Thus, the PCC values for Northern Hemispheric summer season suggest that the simulated precipitation pattern has improved globally and regionally in

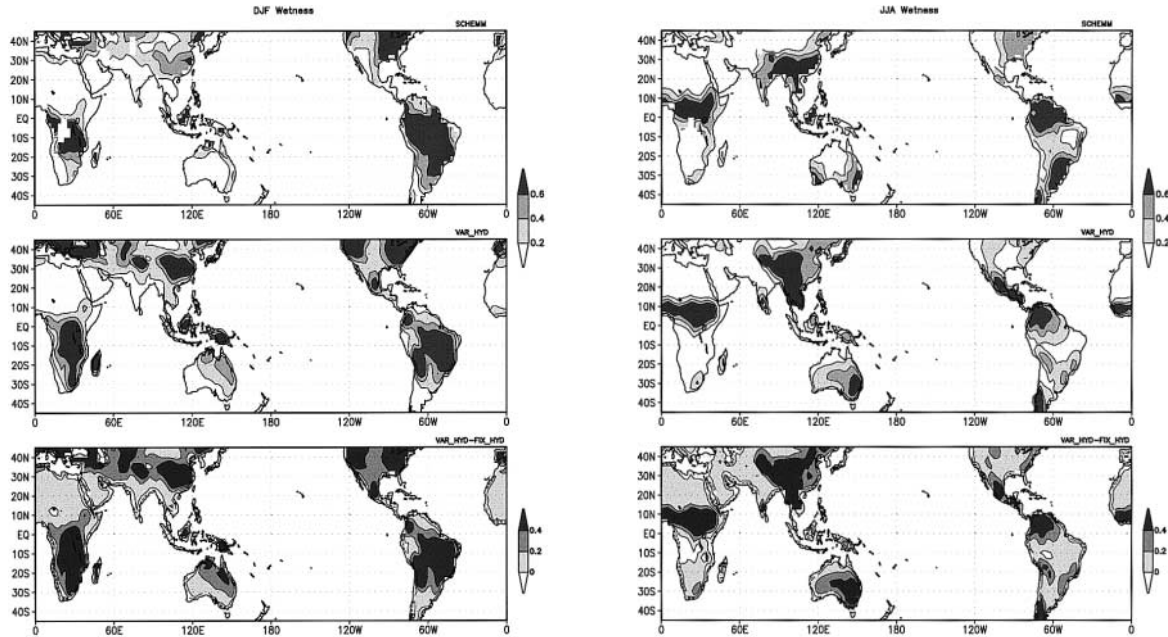


Fig. 6a. Surface Wetness (non-dimensionalised by the field capacity, 15 cm) for DJF season: (top) climatology from the calculations of Schemm et al. 1992, (middle) VAR_HYD and (bottom) difference between VAR_HYD and FIX_HYD simulations.

Fig. 6b. Same as Fig. 6a but for the summer season (JJA).

the VAR_HYD version (except over the three oceanic regions of BOB, SIO and EPAC).

In boreal winter, the simulated precipitation over most of the tropics is correlated better with observation for both simulations compared to that in boreal summer. Significant correlation difference occurs only over the East Pacific (where VAR_HYD simulation is better correlated with the observation) and the South Indian Ocean (where FIX_HYD simulation is better correlated). Over other regions the difference in correlation is small (e.g., Global tropics, SAFR, AUS, WPAC and SAMR). One noticeable feature is the improvement in the East Pacific precipitation simulation by the VAR_HYD version in both the seasons, although the changes in hydrology specification were implemented over the land regions. The precipitation patterns simulated by VAR_HYD is more realistic (in both seasons) than those by the FIX_HYD over most of the tropics.

3.3 Simulation of soil moisture

In the interactive hydrology simulation, soil moisture is allowed to increase whenever rain-

fall exceeds evaporation and vice-versa. In Fig. 6a and Fig. 6b we show the soil wetness (non-dimensionalised with the field capacity) for DJF and JJA respectively. We note that the VAR_HYD reproduces the general features of high wetness over centres of convection such as the African, Indian (peninsular) and the East Asian regions (as compared to the results of Schemm et al. 1992). We also find that during both DJF and JJA, FIX_HYD simulation has lower surface wetness vis-a-vis VAR_HYD. During DJF, the largest impact of evolving surface hydrology is seen to be over southern Africa, Australia, and the American regions and during JJA maximum differences in wetness are seen over equatorial Africa, East Asia and Central American regions. The regions of increased convection activity (Figs. 2a and 2b), such as the equatorial and southern African region, the Australian region during DJF and the peninsular Indian region during JJA are well associated with regions of increased surface wetness (Figs. 6a and 6b) in the VAR_HYD simulation. We note that the wetness over Australia is overestimated (during DJF), and

over the parts of northern India underestimated (during JJA) in the VAR_HYD simulation, when compared with Scheme et al. (1992). However, while comparing with Schemm et al. (1992), it should also be borne in mind that these results are output of a bucket model and not a true observational dataset. Notice that the model systematically underestimates the convection over central India, and overestimates the convection over continental Australia during the respective summer seasons (e.g., simulated seasonal mean OLR patterns shown in Fig. 1 & Fig. 2). These can be due to the multiple interaction among the surface parameters such as the soil moisture, surface temperature and precipitation resulting from different physical parameterizations used in the model.

4. Simulation of seasonal cycle over the Tropics

Simulations of seasonal and intraseasonal variations have been studied by applying harmonic analysis to the observed and simulated OLR datasets. The observed and simulated OLR datasets for each year have been separated into three different classes based on the frequency bands by applying harmonic analysis. The sum of the first four harmonics represents the 'seasonal cycle', (corresponding to time periods up to 90 days) and the sum of 5 to 12 harmonics constitutes the 'intraseasonal cycle', (comprising periods 30 to 70 days) and the residual represents the transient eddies in the harmonic analysis. i.e., for any variable, V ,

$$V(t) = \bar{V} + S(t) + IS(t) + HF(t) + Residual,$$

where,

$$S(t) = \sum_{m=1}^4 V_m \exp\left(i \frac{2\pi m}{T} t\right),$$

$$IS(t) = \sum_{m=5}^{12} V_m \exp\left(i \frac{2\pi m}{T} t\right),$$

$$HF(t) = \sum_{m=13}^{72} V_m \exp\left(i \frac{2\pi m}{T} t\right).$$

Here, \bar{V} represents the annual mean for a particular year, V_m denotes the amplitude of m^{th} harmonic and T is 365 days. $S(t)$ represents the seasonal cycle, $IS(t)$ represents the

intraseasonal cycle, and $HF(t)$ represents the higher frequency components and 'Residual' represents harmonics with timeperiods less than 5 days.

Harmonic analysis was applied to each year separately for both the observed OLR data from 1980 to 1989, and the 10-year simulations of two versions of the model. For assessing the performance of the two versions of the model in simulating the mean climate over the tropics, we had used observed OLR data for the period 1980–1995. But, it was found that the structure of the harmonics were largely insensitive to periods of the OLR data. e.g., the structure was largely similar for the OLR datasets of 1980–1989, and 1980–1995.

To assess the simulation on a smaller spatial scale, different regions have been selected based on seasonal mean amplitudes of observed OLR and centres of organized convection. The selected regions are shown in Fig. 7 and the regions are located over the Monsoon Zone (MZ), Arabian Sea (AS), Bay of Bengal (BOB), South Indian Ocean (SIO), West Pacific (WPAC), East Pacific (EPAC), Northern Africa (NAFR), Southern Africa (SAFR), Australia (AUS) and South America (SAMR). The domain for each box is given in the panel for the model, and for the observation. Harmonic analysis was applied to the box averaged OLR. The reconstructed seasonal cycle in these regions does not exhibit much year to year variation. Figure 8 shows the observed and simulated mean seasonal cycle for all the ten regions. Based on harmonic analysis, monsoon onset (in the Monsoon Zone, denoted by MZ) can be identified with a change in sign of $S(t)$ from dry winter phase (positive) to wet summer phase (negative) (Murakami et al. 1986). The withdrawal occurs with the phase transition from negative to positive. In Fig. 8 we have shown the mean of the 10 years of the first four harmonics for the individual years. For the model, temporal standard deviation of the seasonal cycle is very small, and the analysis of the mean of the 10 years seasonal cycle (Fig. 8) can be justified (though there exists a slight year to year variation in the onset which corresponds to the time at which $S(t) = 0$). In Fig. 8, the solid line represents the observation, the dashed line is for variable hydrology simulation, and the dotted line is for fixed hydrology simulation. Over the

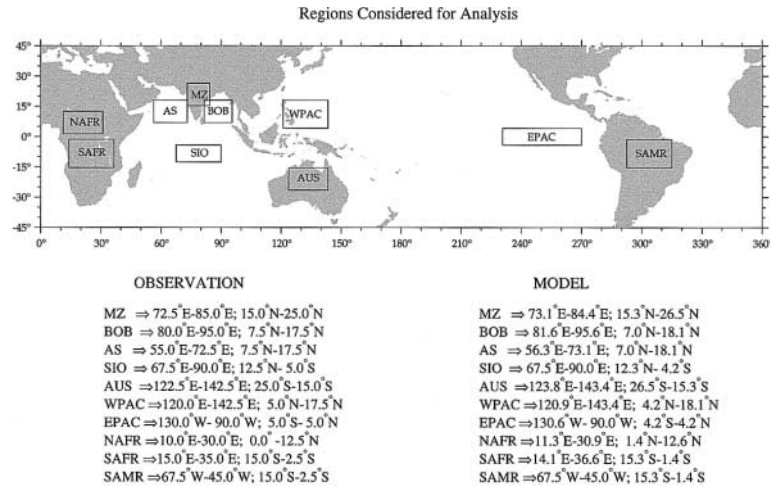


Fig. 7. The regions selected for power spectrum analysis. The domain for each region (denoted by respective abbreviation) is given for observation and model.

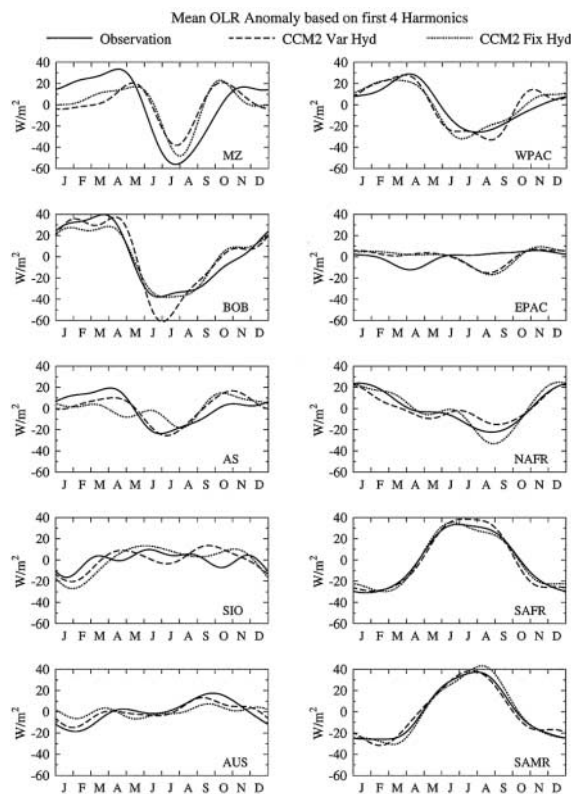


Fig. 8. Observed and simulated 10 year mean seasonal cycle $[S(t)]$ for the 10 regions showed in Fig. 7.

oceanic regions, and over the monsoonal regions corresponding to the Monsoon Zone over India, Australia and North Africa the simulations not only vary from the observation, but differ from each other as well.

Over the Monsoon Zone (MZ), both the simulations have late onset and early withdrawal of Indian summer monsoon. In addition, there exists a lag in the time of occurrence of the peak between the simulations. Over the Bay of Bengal (BOB), the simulation of the onset in the fixed hydrology case is in better agreement with the observation. But, over the Arabian Sea (AS), the simulation of seasonal mean precipitation (and also the onset), is more realistic for the variable hydrology case. Over these two regions, the models have a tendency to simulate early withdrawal of monsoon. Over the South Indian Ocean (SIO), the simulations are out of phase, and differ in amplitude compared to the observation. On the contrary, over the West Pacific (WPAC) the simulations show an early onset and early withdrawal compared to observation. But, the phase of the seasonal cycle simulated by fixed hydrology case is closer to the observation. Over Australia (AUS), South Africa (SAFR) and South America (SAMR), both the models are in good agreement with the observation. The simulations are out of phase with the observation during spring and autumn over the EPAC region.

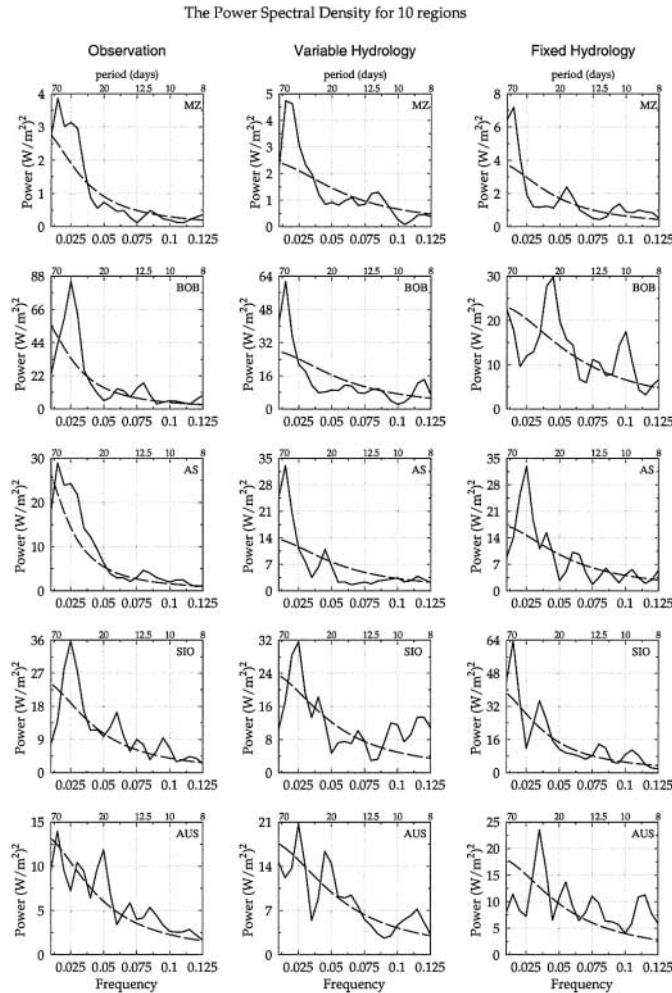


Fig. 9. The power spectral density (solid curves) of daily OLR anomalies for the 10 regions. The spectra are for the 10 year average of OLR (after detrending) anomalies for each region. The corresponding red noise spectra (dotted curves) are also shown.

5. Simulation of intraseasonal variability over the Tropics

5.1 Power spectrum analysis

Power spectrum analysis of OLR has been performed to identify the impact of surface hydrology on the simulation of intraseasonal variation. The power spectrum analysis has been conducted by considering harmonics beyond wavenumber three (i.e., wavenumbers 0, 1, 2 and 3 corresponding to the annual and seasonal cycles are not considered). Power spectrum analysis has been applied to all the ten regions for which the results of harmonic analysis were presented in the last section. The

spectrum of ‘red noise’ is computed based on lag-one auto correlation (Mitchell et al. 1966). Figure 9 shows the power spectra of the 10 year averaged daily OLR for the 10 regions analysed. The averaged spectra of observed, and simulated (by both models) OLR anomalies, show dominant spectral peaks above the respective red noise spectra in the 20–70 day time scales in all the 10 regions, except over SAFR for the fixed hydrology simulation. Over two regions i.e., AS and SIO, the spectral peak for the variable hydrology simulation matches well with the observation. Since there is large fluctuation from year to year in the intraseasonal scales, we have shown the significant

The Power Spectral Density for 10 regions

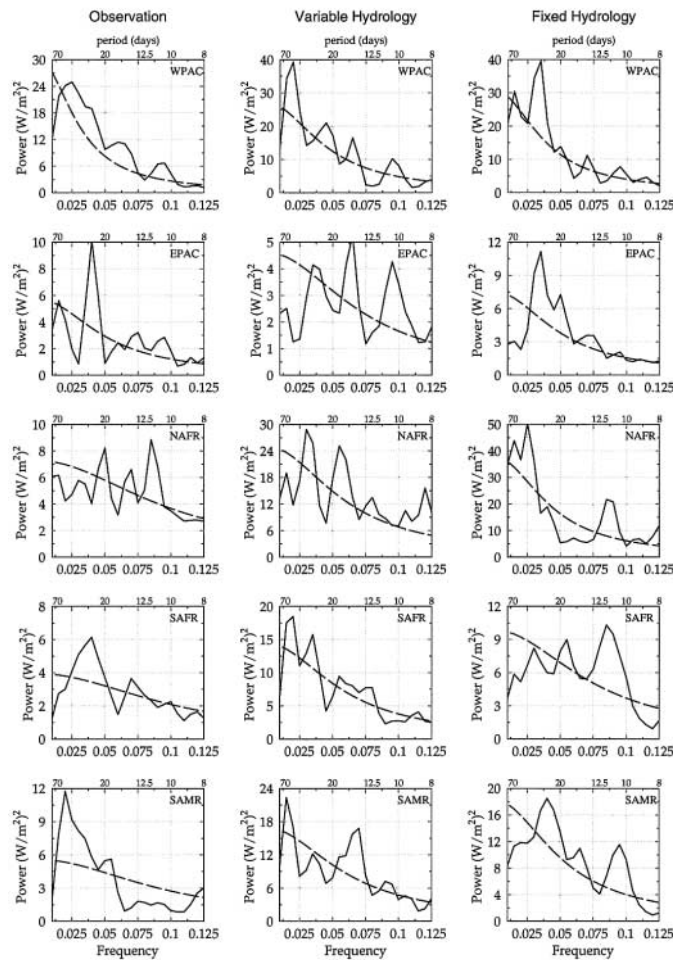


Fig. 9 (continued)

spectral peak for both VAR_HYD, and FIX_HYD simulations for each of the individual years in Fig. 10. We note that over MZ, the role of variable hydrology is to increase the energy in intraseasonal time-scale (20–70 days) vis-a-vis the fixed hydrology (Fig. 10, the significant peak for individual years for the FIX_HYD simulation is above 70 days in most of the years). Over Australia (AUS), two spectral peaks around 60 and 20 days are captured by the variable hydrology simulation which are nearly absent in the fixed hydrology simulation (FIX_HYD showing peaks around 25 days and 16 days, Fig. 9). Over the BOB, the variable hydrology simulation has a spectral peak corresponding to slightly lower frequency compared to the observation, but the power asso-

ciated with the primary peak is comparable. Generally, over the warm oceanic regions the dominant peak shifts towards lower frequency in the variable hydrology simulation (compared to the fixed hydrology simulation), and becomes closer to the observation (e.g., the BOB & WPAC). Thus, over land regions the role of interactive hydrology is to transfer energy into the 20–70 day time-scale, while over oceanic regions (BOB & WPAC) it is to move the spectral peak to lower frequencies. The simulation by the variable hydrology case is much closer to observation when compared to the fixed hydrology case over all the continental regions (MZ, SAMR, NAFR, SAFR). Over the Monsoon Zone, the fixed hydrology simulation does not show a spectral peak in 20–70 days in any of

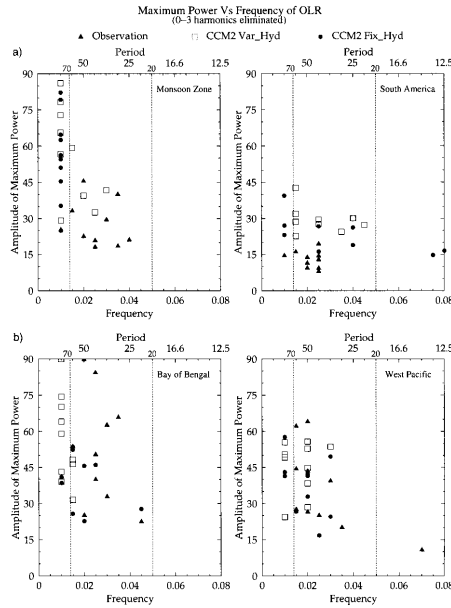


Fig. 10. The frequency corresponding to the significant maximum power of observed and simulated OLR (in the time series of 10 years) over a) the land regions of Monsoon Zone (MZ) and South America (SAMR), and b) the oceanic regions of the Bay of Bengal (BOB) and West Pacific (WPAC).

the years (Fig. 10). Whereas, the variable hydrology version of the model simulates significant intraseasonal peak in 4 years, and a significant peak is found in this interval for 9 years in the observation.

It is interesting to note that while FIX_HYD had simulated the seasonal cycle quite realistically over BOB (Fig. 8), on the intraseasonal scale VAR_HYD simulates more realistically the variation both in amplitude and periodicity, with a peak around 40 days (Fig. 10). Over the North African region low-frequency variability (30–70 day timeperiods) is low in the observations (Fig. 9). The high frequency (less than 20 days) variability is much lower in the FIX_HYD case, while the secondary peak in the VAR_HYD is closer to the observed values of around 15 days. In SAFR and AUS, soil moisture variation introduces a peak at the lower frequencies as compared to the fixed hydrology simulation. In contrast, over Northern Africa (NAFR) it introduces a peak at the higher frequency.

Over the West Pacific too, variable hydrology performs better than the fixed hydrology simulation, the dominant one with the spectral peak at around 60 days, which is close to the observed peak at 70 days; in contrast the fixed hydrology simulation has a peak around 30 days. Even over the Southern Indian Ocean (SIO), a predominantly oceanic region (where impact of surface hydrological surface involving variation in soil moisture is expected to have the least impact) shows significant improvement in the amplitude of the dominant peak (reduced by almost 50% in the VAR_HYD case in contrast to the FIX_HYD case). In summary, the impact of surface hydrological changes has been found over both the continental regions, and oceanic regions in the seasonal as well as in the intraseasonal variation.

5.2 Wavenumber-frequency spectral analysis

In the previous section we have studied the intraseasonal variation as an averaged quantity over a region without specific reference to the nature of these variations, i.e., whether these are standing oscillations, zonally propagating waves or meridionally migrating convective systems. In this section we study the impact of surface hydrological variations on the equatorially trapped, eastward migrating waves, such as the Madden Julian Oscillation.

The space-time spectral technique is useful for the study of the zonally propagating waves as it decomposes a variable dependent on time and longitude into wavenumber (spatial), and frequency (temporal) components for eastward and westward propagating waves as well as zonal mean fluctuations (Hayashi 1982). The procedure and the algorithm for the space-time spectral analysis is explained in detail by Hayashi (1977, 1982). The data sets are seasonally detrended before applying the space-time spectral analysis. This was done by first generating the 10 year mean for each day of the annual cycle, and then computing the annual mean and the first three harmonics from this time series. The mean, and the first three harmonics were then removed from the 10 year time series. The space-time power spectral analysis is applied to OLR from observation and the simulations. The spectral power density is computed for each year using the anomaly data averaged between 10°S–10°N.

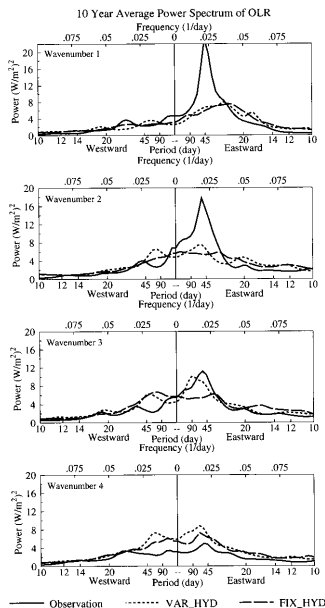


Fig. 11. Average wavenumber-frequency spectra for 10°S – 10°N OLR from observation (NOAA), from variable and fixed hydrology simulations for wavenumbers 1 to 4.

The average space-time spectra for wavenumbers 1–4 in observed and simulated OLR are shown in Fig. 11. The average spectra for observed OLR were estimated by excluding years with a secondary higher period spectral maximum for wavenumber 2. In some years, large variance occurs at the higher period (greater than 90 days) as a secondary maximum corresponding to the spatial scale of wavenumber 2 in observed OLR spectrum. It is to be noted that the NOAA satellites were occasionally unable to provide OLR observations for certain periods of the year (e.g., in year 1992 & 1994). These missing values have been filled by linear interpolation in OLR observations, using the preceding and succeeding days measurement (Liebmann and Smith 1996). We have found that the large variance for wavenumber 2 at higher periods occur during these years due to this interpolation in the observed NOAA (interpolated) OLR dataset. Hence, we have excluded these years (1992 & 1994) from our analysis.

For wavenumber 1, while observation shows a peak in the 35–45 day time-scale, both fixed

and variable hydrology simulations show an eastward peak in this timescale, though the energy is much smaller. It is also interesting to note that while in observations the maximum energy is at wavenumber 1, and reduces rapidly at higher wavenumbers, the energy at wavenumbers 1, 2 and 3 are comparable in the two simulations. The energy in wavenumbers 1 and 2 in the simulations are much smaller than that in the observations. In wavenumber 3, VAR_HYD has a eastward peak at around 90 days, and westward peak at about 45 days, while FIX_HYD has only a westward peak. Both the simulations have higher power at higher wavenumbers vis-a-vis observations.

5.3 Characteristics of equatorially trapped eastward propagating modes

Global eastward propagations associated with the Madden Julian Oscillation (MJO) constitute one of the major components of intraseasonal variation. The simulation of the primary characteristics of MJO has been studied using longitude-time cross section of OLR, averaged between 10°S – 10°N for the 10 year period. Since the seasonal cycle dominates the field, the observed and simulated datasets are seasonally detrended. This was done by first generating the 10 year mean for each day of the annual cycle. Then computing the annual mean, and the first three harmonics, from this time series. The mean and the first three harmonics were then removed from the 10 year time series. Further, a 120 point, 20–70 days band pass Lanczos filter (Duchon 1979) was applied to isolate intraseasonal time scales.

Figure 12 compares the Hovmöller diagram of OLR for a representative year (year with prominent propagations) from the VAR_HYD and FIX_HYD simulations with observation. The negative anomalies ($< -5 \text{ W m}^{-2}$ is shaded) denote enhanced convection and positive anomalies denote reduced convection. In observation, the enhanced convection originates from the western Indian Ocean, and moves towards the central Pacific and decays over the colder SST regions east of the dateline. These anomalies show much slower, or little eastward migration over central to eastern Pacific. In observation, the intraseasonal activity is more pronounced during the Northern Hemispheric winter and spring, with coherent

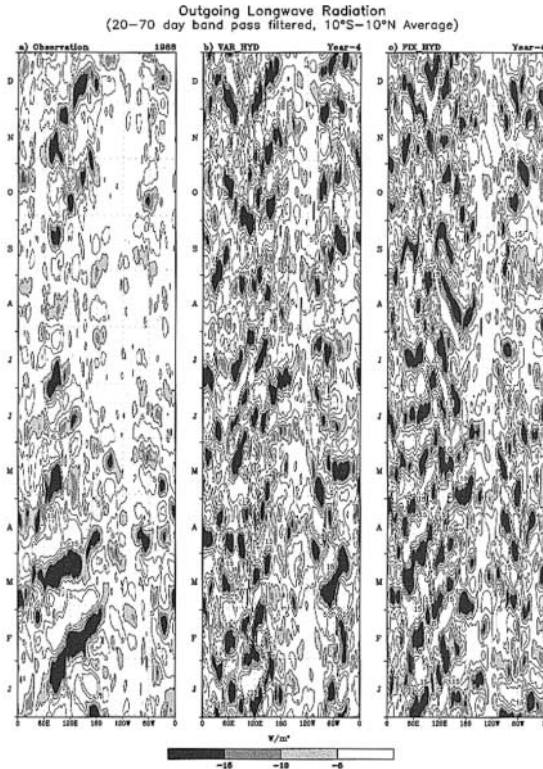


Fig. 12. Hovmöller diagram of 20–70 day band pass filtered daily OLR averaged over 10°S–10°N from: a) Observation; b) VAR_HYD; and, c) FIX_HYD simulations.

eastward propagations of organized convection compared to the summer. This seasonal behaviour of the MJO has been explained by Salby et al. (1994) in terms of the response of the atmosphere to the latitudinal position of the tropical heat sources.

The longitude-time patterns for the models show that the propagations in both simulations are faster, and are not as continuous, as the observed propagation in the zonal direction. This is consistent with the findings of previous studies (e.g., Park et al. 1990; Slingo et al. 1996) that the models which have a reasonably realistic simulation of MJO, have relatively more power at higher frequencies than the observed. Also, the simulations capture the slowing down of eastward propagations around the date line. Despite being forced with climatological SST, the simulations show year to year

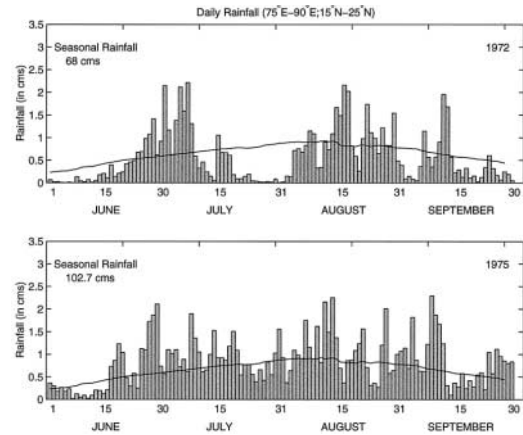


Fig. 13a. Daily observed IMD rainfall averaged over central India for two representative years (1972 and 1975). The solid line represents the daily long-term mean.

variation in the propagation characteristics of MJO.

The propagations in the fixed hydrology case are discontinuous, and there are some westward propagations between 30°E–90°E. Also, in the variable hydrology case, there are some events of continuous eastward propagations. Although both the simulations fail to show any clear seasonality in the MJO activity, there is a weakening of eastward propagation in the variable hydrology case during summer. It was seen that in the wavenumber-frequency spectra of fixed hydrology version, there was some power at intraseasonal time scales associated with westward moving waves (Fig. 11).

6. Intraseasonal variation over the Indian region

Organized convection over the Indian region exhibits intraseasonal variation. Over the heated continental landmass there exist active-break cycles in precipitation. Gadgil and Asha (1992) have shown that these active-break cycles can have a strong impact on the seasonal mean precipitation being above, or below, normal. The daily central Indian rainfall, based on the IMD data in Fig. 13a, shows that the below-normal monsoon of 1972 is characterised by long breaks while there are fewer breaks in the above-normal monsoon of 1975. Since these active-break cycles in organized convection

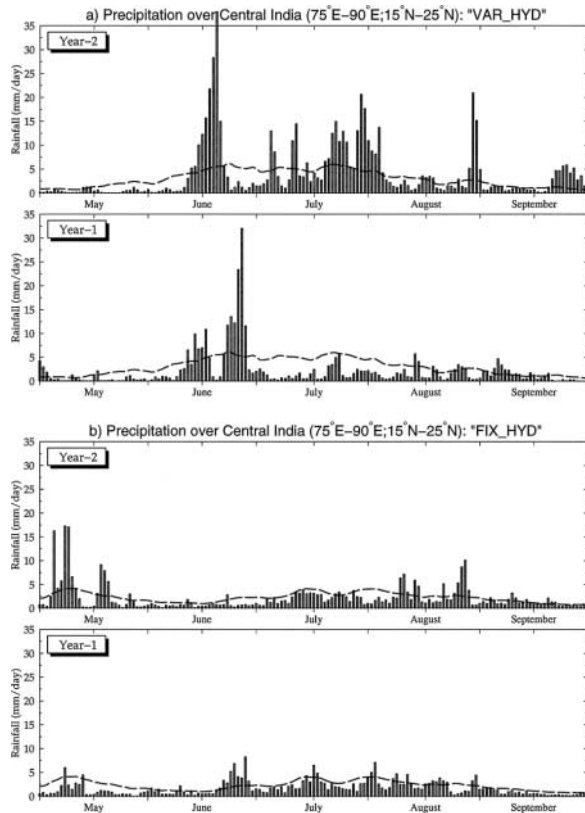


Fig. 13b. Simulation of daily precipitation over the central Indian region by a) VAR_HYD and b) FIX_HYD simulations. The dashed line represents the 10 year daily mean for the respective simulation.

occur over the continental region, it is necessary to examine the role of surface-hydrological feedbacks in modulating organized convection on the intraseasonal time-scales. Polcher (1995) has suggested that the role of surface hydrological changes is to modify the frequency of occurrence of organized convection, rather its magnitude. Their study however, did not include the Indian summer monsoon region. However, our spectral analysis (Figs. 9 and 10) suggests that both magnitude and frequency could be affected by the change in the surface hydrology specification.

Examining the daily rainfall over the central Indian region (75°E – 90°E , 15°N – 25°N), we notice (Fig. 13b) that while the VAR_HYD simulation shows higher intraseasonal activity, the

same appears to be attenuated in the FIX_HYD case. In the FIX_HYD simulation we notice only one or two epochs of strong precipitation during a season. In contrast there appear to be more spells of intense rainfall in the VAR_HYD simulation. Other years of simulation also appear to have a very similar pattern. The VAR_HYD simulation appears to capture the active-break cycles over the central Indian region, than the FIX_HYD simulation. We have shown the precipitation for two representative years of the two simulations (Fig. 13b). Similar patterns are repeated in almost all the other years of these simulations (i.e., VAR_HYD simulates much more vigorous intraseasonal activity than the FIX_HYD simulation).

The super-synoptic scale rainfall fluctuation in VAR_HYD is a persistent feature in all 10 years. In addition, there are also realistic year to year variation in the distribution of daily rainfall within a season. This is evident from the difference between the two years shown in Fig. 13b. The daily 10-year mean (dashed curve) is also different compared to those for the two years. Whereas for FIX_HYD, the distribution of rainfall is almost similar for the two years, and the daily long term mean. There is not much difference in the daily rainfall during the pre-monsoon season and the monsoon season. This difference between the two simulations is related to the fact that in variable hydrology the soil moisture is allowed to vary with the rainfall. It was found that the intraseasonal variation in VAR_HYD is similar to that obtained when the model is forced with schemm soil moisture climatology (not shown). It was also found from additional experiments that the intraseasonal variation over the monsoon zone is not improved by fixing the soil moisture at a higher value alone (not shown).

While the precipitation pattern over the central Indian region (Figs. 13a and 13b) clearly shows the presence of considerable intraseasonal activity, the same cannot be perceived from the averaged power spectrum of Fig. 9. While comparing the two, we should bear in mind that while the active-break cycle exists only during the months of strong convective activity (i.e., JJA period), the peak of the spectrum shown in Fig. 9 represents variations over the entire year, and is the average of the spectra over the 10-year period. How-

ever, we do find that peaks in the intraseasonal frequencies are noticeable in individual years (Fig. 10), whose magnitude is reduced due to averaging over the 10-year period in Fig. 9.

6.1 Meridional propagation of convective zones

The monsoon over South Asia is one of the most vigorous and energetic large scale weather phenomenon and has a major impact on the global circulation during the northern summer. In addition to the pronounced seasonal cycle, the thermal contrast between the Asian continent, and the adjacent Indian and Pacific Oceans and the typical orographic features are also responsible for the formation and maintenance of the Asian summer monsoon. The monsoon is thus closely linked to the seasonal cycle, and displays remarkable spatial and temporal consistency. Despite this consistency of the seasonal cycle, there is substantial intraseasonal variability in its strength. This intraseasonal variability may affect the monthly or seasonal mean of the monsoon for any particular year (Gadgil and Asha 1992). Over the Indian region, the active-break cycles, which characterise the monsoon intraseasonal variability, are associated with two preferred locations of the TCZ (Tropical Convergence Zone), one over the continent and another over the equatorial Indian Ocean (e.g., Sikka and Gadgil 1980; Yasunari 1979). Related to the transition from the oceanic to the continental regime, northward propagation of the oceanic TCZ has been observed and widely studied (Yasunari 1979, 1981; Sikka and Gadgil 1980; Krishnamurti and Subrahmanyam 1982). Over the Indian region, in general, northward propagations of the oceanic TCZ leading to a revival of the continental TCZ occur at intervals of 2–6 weeks. Poleward propagations account for about 50% of revival of the continental TCZ from break condition. This phenomenon is considered to be a regional component of the global eastward propagation (e.g., Julian and Madden 1981; Wang and Rui 1990). During boreal winter, the equatorial eastward propagation dominates, whereas during boreal summer the northward propagations in the Indian and western Pacific regions, (along with westward propagation in the western Pacific off-equatorial region) are more active.

The northward propagations of coherent convective structures from the equatorial oceanic zone to the continent over the Indian longitudes has also been investigated by various theoretical studies. Pioneering studies by Webster and Chou (1980a, b), and Webster (1983) identified that the ground hydrology as a crucial factor in generating intraseasonal variation of the Tropical Convergence Zone (TCZ) in a simple phenomenological climate model. Gadgil and Srinivasan (1990), and Srinivasan et al. (1993), modified this model to make the simulation more realistic and studied the sensitivity of the period of the propagating events to the specification of ground hydrology. They suggested that the poleward gradient of vertical instability rather than surface hydrological effects to be the prime cause of poleward propagations. Nanjundiah et al. (1992) investigated the sensitivity of simulation of poleward propagations, and the length of the active phase over the continental region to the model's dynamical system, and to surface hydrological effects.

Figure 14 shows time-latitude diagram of observed GPCP precipitation along 95°E for a representative year (1997). Similar structure of intraseasonal variation have been observed over the Indian region during the monsoon season of almost all the years (Sikka and Gadgil 1980). Substantial intraseasonal variability is noted in the precipitation with the rainbelt making successive propagations from the oceanic zone to the heated continent. The evolution and intensity of the precipitation events exhibit difference from year to year.

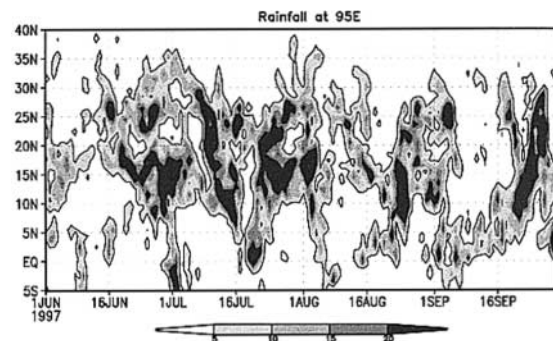


Fig. 14. Time latitude diagram of GPCP precipitation over 95°E for a representative year (1997).

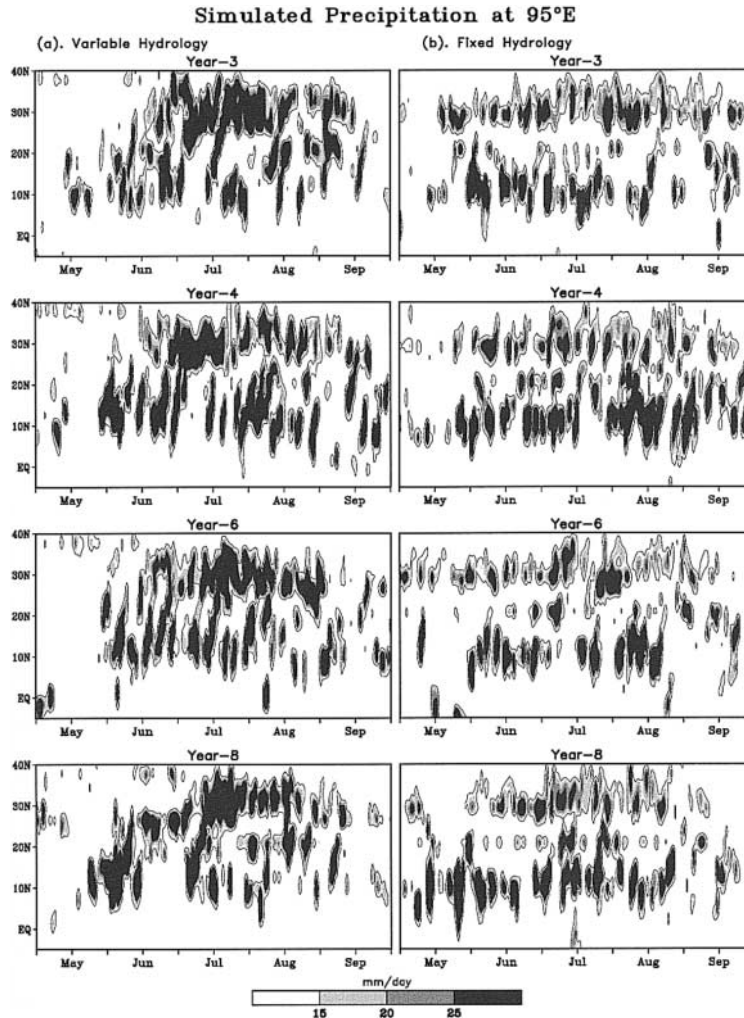


Fig. 15. Time-latitude diagram of precipitation over 95°E for different years simulated by the model with a) variable hydrology and b) fixed hydrology. The lowest contour represents 10 mm day⁻¹.

Figure 15 shows the diagram of simulated precipitation over 95°E for four different years. In variable hydrology simulation there are clear northward propagations of rainbelts which are prevalent and active during the monsoon season. An important feature in the variable hydrology simulation is the persistence of the rainbelt over the continent until the occurrence of a northward shift of the rainbelt from the oceanic zone. In the fixed hydrology simulation, coherent poleward propagation are not simulated, instead persistent rainbelts occur over two preferred locations, one around 10°N and another around 30°N, without much interaction between them during the whole season.

a. Time-lagged correlations

In order to distinguish the northward propagating events from other components of intraseasonal variation, time-lagged correlations of precipitation (averaged between 92.5°E–97.5°E) between each individual point and all the other points in the latitudinal band 5°S–35°N, were computed for the simulations. Figure 16 shows the time lagged correlation of simulated precipitation at the point 12°N with all the other points for a representative model year-4. In the variable hydrology simulation (Fig. 16a), the northward tilting of the positive correlation area indicates northward propagation. The average speed of propagation is about

Time-Lagged Correlation with Precipitation at 12°N

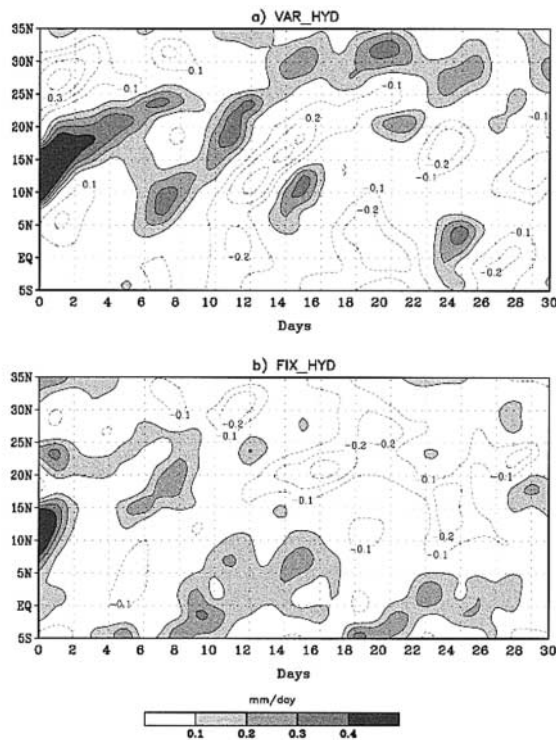


Fig. 16. The time-lagged correlation of precipitation at the point 12°N with all the points in the latitudinal band 5°S–35°N for a) variable hydrology and b) fixed hydrology simulations averaged over 92.5°E–97.5°E.

twice as fast as the observed speed of about 1°/day (as estimated by Gadgil (1990) based on OLR observations). The time-lagged correlation for other years (not shown) also show clear northward propagation over the latitudinal belt between 7°N and 20°N in the variable hydrology case. Similar time lagged correlation pattern, for fixed hydrology simulation (Fig. 16b), shows an area of negative correlation near to 10°N at initial lead times (just after lead time of two days). This implies the absence of clear meridional propagation in this version of the model. Thus, the simulation of meridional propagation in the model is found to be strongly dependent on the treatment of surface hydrology in the model, with the interactive hydrology improving the meridional propagations over the Indian longitudes.

6.2 Intraseasonal variations and moist static energy

Webster (1983) suggested that the poleward gradient of sensible heat flux was the principal cause of northward propagations of the cloud-bands. However, Gadgil and Srinivasan (1990), and Nanjundiah et al. (1992) showed that poleward propagations occurred even in the absence of poleward gradient of sensible heat flux and that the poleward gradient of stability (poleward region being less vertically stable than the region equatorward of the convective band) caused poleward propagations in their model. Srinivasan et al. (1993) have shown using ECMWF analysis that such gradients occur in observations also. The major reason for the occurrence of this is the increase in moisture in the lower layers of the atmosphere, which changes the vertical stability profile from strongly stable during the pre-monsoon season, to near-neutral during the monsoon period (and thus more amenable to convection). Hence moist static enthalpy in the lower troposphere is a good measure of vertical stability.

The latitudinal variation of vertically integrated (over 1000–400 hPa) moist static energy (m_l) averaged over a longitudinal band during the time of an active northward propagation, have given further insight on the absence of northward propagations in the FIX_HYD simulation. Figure 17 shows the latitudinal variation of observed (based on NCEP/NCAR reanalysis) and simulated (by VAR_HYD and FIX_HYD simulations) m_l averaged over 92.5°E–97.5°E during a given month (when both the observation and the VAR_HYD simulation have the meridional propagations). The major difference between the latitudinal variation of m_l from the fixed and variable hydrology simulations (which is similar to the observed variation) is the absence of meridional variation of m_l over a latitudinal band from 10°N–25°N in the fixed hydrology version. Higher m_l implies a larger amount of water vapour in the lower troposphere which is favourable for sustaining stronger convection. The presence of counter gradient of m_l over a region (as in the case of fixed hydrology simulation) causes it to be less conducive for the poleward movement of convective zones over that region.

Vertically Integrated Moist Static Energy (1000-400 hPa) ave. around 95°E

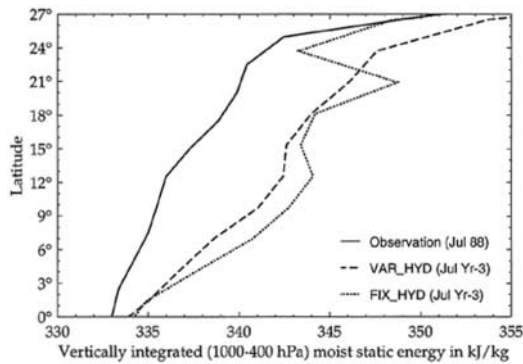


Fig. 17. The latitudinal variation of vertically integrated moist static energy (in the layer 1000–400 hPa) averaged over 92.5°E–97.5°E in a given month (when an active propagating event exists) from: NCEP/NCAR reanalysis; VAR_HYD; and, FIX_HYD simulations.

6.3 Meridional propagations over the western Pacific

Srinivasan and Smith (1996) have shown that meridional propagations of organized convection is a feature that is not unique to the Indian longitudes, but occurs over other tropical regions such as the western Pacific (120°E–140°E). Comparing MSU rainfall with simulations from VAR_HYD and FIX_HYD schemes, we notice that (Fig. 18a) observed rainbands originate near the equatorial western Pacific and quickly propagate polewards. The latitudinal variation of vertically integrated moist static energy (in the layer 1000–400 hPa) over the West Pacific region (averaged over 120°E–140°E) is shown in Fig. 18b for a representative month. Over this region, northward propagation of convective bands was found to occur throughout the year. Consistent with the latitudinal variation of precipitation, m_l increases with the latitude for FIX_HYD simulation. There is a counter gradient for VAR_HYD simulation limiting the propagations after around 15°N.

7. Conclusions

In this paper, the effect of surface hydrology specification by two versions of the NCAR CCM2 model, which differ in the treatment of surface hydrology, has been studied. The two

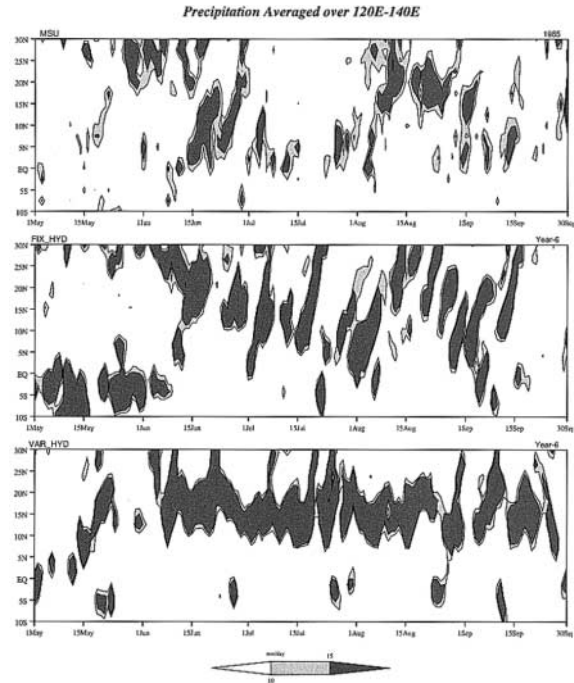


Fig. 18a. Time-latitude diagram of precipitation (mm/day) over western Pacific (120°E–140°E) for: a) observation; b) VAR_HYD; and, c) FIX_HYD simulations during the northern summer season.

Vertically Integrated Moist Static Energy (1000-400 hPa) averaged over 120°-140°E

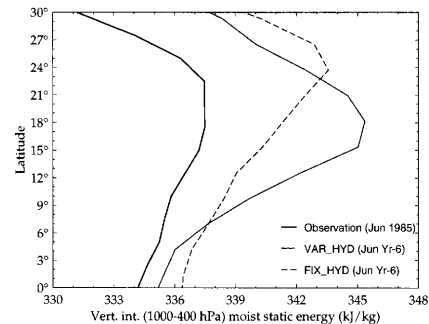


Fig. 18b. The latitudinal variation of vertically integrated moist static energy (in the layer 1000–400 hPa) averaged over 120°E–140°E for a given month from: NCEP/NCAR reanalysis; VAR_HYD; and, FIX_HYD simulations.

ten year climate simulations (first with an interactive surface hydrology, VAR_HYD and the second with hydrology fixed to annual climatological values, FIX_HYD) showed that the model captures the locations of major centers of convection and circulation over the tropics. On regional scale, during boreal summer, the simulations of mean convection showed marked difference between the two simulations, and hence demonstrated the impact of surface hydrology specification. During boreal winter, the impact of surface hydrology was found to be less. During both DJF and JJA, annual mean surface wetness prescribed in the FIX_HYD simulation, is lower than wetness simulated by VAR_HYD.

It was found that the impact of surface hydrology specification was not entirely local in the model as seen in the difference patterns of OLR and precipitation (Fig. 2c). The changes in the surface hydrological interactions over continental regions appeared to affect the circulation and precipitation patterns over other parts of the tropics. The difference patterns of precipitation, circulation, and VMS between the two simulations were seen to be closely associated, i.e., regions with higher precipitation in one of the simulation had lower VMS and higher ascent at 500 hPa (and vice-versa). This association and the non-local nature of impact of soil hydrology was explained through changes in moist static energy budget using the simple model of Neelin and Held (1987).

Harmonic analysis of simulated OLR revealed the model's ability to simulate the seasonal convective centers. The impact of specification of hydrology on the evolution of the seasonal cycle was found to be large over the Asian summer monsoon region (especially over the Bay of Bengal and the Monsoon Zone, Fig. 8). The fixed hydrology version simulated the seasonal cycle more realistically than variable hydrology simulation over the Bay of Bengal. We notice that the impact of changes in surface hydrology specification is not similar over all the regions. In certain regions higher frequencies are introduced, while in certain other regions lower frequencies become prominent, with the introduction of interactive soil hydrology.

The active-break cycle in precipitation over the central Indian region could be simulated

only with interactive surface hydrology. Simulation of meridional propagations of convective zones over the Indian region were more realistic in VAR_HYD. The variable hydrology version was able to simulate all the major features such as: the amplitude of the meridional migration; the persistence of convective bands for a short time when it reaches the northern most location; and, occurrence of coherent propagations only during the summer season. The active-break cycles over the Central Indian region were also realistically simulated by the VAR_HYD simulation. The simulated meridional propagation of precipitation was found to be faster than the observed meridional propagation. The ability of VAR_HYD to simulate poleward propagations were associated with latitudinal gradient of vertical stability. VAR_HYD simulations and observations showed decreased poleward vertical stability, while FIX_HYD simulated a counter-gradient not favourable for poleward propagation. In contrast, we find that poleward propagations were more noticeable in the FIX_HYD simulation over the western Pacific region. We also find that specification of surface hydrology over continental regions has little impact on the simulation of MJO. The specification of surface hydrology over the continental regions has a significant impact on the simulation of tropical climate in both continental and oceanic regions on both seasonal and intraseasonal scales.

Acknowledgments

The authors thank the Chairman SERC-IISc for providing the computational facilities on the SP2 parallel computer. They thank Dr. H. Hendon of CIRES (Co-operative Institute for Research in Environmental Sciences) for providing the daily interpolated OLR data. This work was supported by Department of Science & Technology, Govt. of India under grant ES/48/004/97. The parallel version of CCM2 used in this study was developed at Argonne and Oak Ridge National Laboratories under the US DoE CHAMMP (Computer Hardware and Advanced Mathematical Modelling Program for climate studies) and the use of the same is gratefully acknowledged. The valuable and perceptive comments of the two referees which helped in improving the paper substantially are also gratefully acknowledged.

References

- Bras, R.L., 1999: A brief history of hydrology. *Bull. Amer. Meteor. Soc.*, **80**, 1151–1164.
- Drake, J., I. Foster, J. Michalakes, B. Toonen and P. Worley, 1995: Design and performance of a scalable parallel Community Climate Model. *Parallel Computing*, **21**, 1571–1592.
- Duchon, C.E., 1979: Lanczos filtering in one and two dimensions. *J. Appl. Meteor.*, **18**, 1016–1022.
- Gadgil, S., 1990: Poleward propagations of the ITCZ: Observations and theory. *Mausam*, **41**, 285–290.
- and G. Asha, 1992: Intraseasonal aspects of the Indian summer monsoon I: Observational aspects. *J. Meteor. Soc. Japan*, **70**, 517–527.
- and J. Srinivasan, 1990: Low frequency variation of tropical convergence zone. *Meteor. Atmos. Phys.*, **44**, 119–132.
- Goswami, B.N., 1998: Interannual variations of Indian summer monsoon in a GCM: External conditions versus internal feedbacks. *J. Climate*, **11**, 501–522.
- Gruber, A. and J.S. Winston, 1978: Earth-atmosphere radiative heating based on NOAA scanning radiometer measurements. *Bull. Amer. Meteor. Soc.*, **59**, 1570–1573.
- and A.F. Krueger, 1984: The status of the NOAA outgoing longwave radiation data set. *Bull. Amer. Meteor. Soc.*, **65**, 958–962.
- Hack, J.J., B.A. Boville, B.P. Briegleb, J.T. Kiehl, P.J. Rasch and D.L. Williamson, 1993: Description of the NCAR Community Climate Model (CCM2). *NCAR Tech. Note, NCAR/TN-382+STR, NTIS PB93-221802/AS, Natl. Cent. for Atmos. Res.*, Boulder, Colo., 108pp.
- , J.T. Kiehl, P.J. Rasch and D.L. Williamson, 1994: Climate statistics from the National Centre for Atmospheric Research Community Climate Model CCM2. *J. Geophys. Res.*, **99**, 20,785–20,813.
- Hahmann, A.N., D.M. Ward and R.E. Dickinson, 1995: Land surface temperature and radiative fluxes response of the NCAR CCM2/Biosphere-atmosphere transfer scheme to modifications in the optical properties of clouds. *J. Geophys. Res.*, **100**, 23,239–23,252.
- Hayashi, Y., 1977: Space-time power spectral analysis using the maximum entropy method. *J. Meteor. Soc. Japan*, **55**, 415–420.
- , 1982: Space-time spectral analysis and its application to atmospheric waves. *J. Meteor. Soc. Japan*, **60**, 156–171.
- Holloway, J.L. and S. Manabe, 1971: Simulation of climate by a global general circulation model. 1. Hydrologic cycle and heat balance. *Mon. Wea. Rev.*, **99**, 335–370.
- Huffman, G.J., R.F. Adler, M.M. Morrissey, S. Curtis, R. Joyce, B. McGavock and J. Susskind, 2001: Global precipitation at one-degree daily resolution from multi-satellite observations. *J. Hydrometeor.*, **2**, 36–50.
- Joseph, P.V. and J. Srinivasan, 1999: Rossby waves in May and the Indian summer monsoon rainfall. *Tellus*, **51A**, 854–864.
- Julian, P.R. and R.A. Madden, 1981: Comments of a paper by T. Yasunari, a quasi-stationary appearance of 30 to 40 day period in the cloudiness fluctuations during the summer monsoon over India. *J. Meteor. Soc. Japan*, **59**, 435–437.
- Kalnay, E. and Co-authors, 1996: The NCEP/NCAR 40-year reanalysis project. *Bull. Amer. Meteor. Soc.*, **113**, 2158–2172.
- Kiehl, J.T., J.J. Hack and B.P. Briegleb, 1994: The simulated Earth radiation budget of the NCAR CCM2 and comparisons with the Earth Radiation Budget Experiment (ERBE). *J. Geophys. Res.*, **99**, 20,815–20,827.
- Krishnamurti, T.N. and D. Subrahmanyam, 1982: The 30–50 day mode at 850 mb during MONEX. *J. Atmos. Sci.*, **39**, 2088–2095.
- Lieberman, R.S., C.B. Leovy, B.A. Boville and P. Briegleb, 1994: Diurnal heating and cloudiness in the NCAR Community Climate Model (CCM2). *J. Climate*, **7**, 869–889.
- Liebmann, B. and C.A. Smith, 1996: Description of a complete (interpolated) outgoing longwave radiation dataset. *Bull. Amer. Meteor. Soc.*, **77**, 1275–1277.
- Manabe, S., J. Smagorinsky and R.F. Strickler, 1965: Simulated climatology of a general circulation model with a hydrologic cycle. *Mon. Wea. Rev.*, **93**, 769–798.
- Mitchell, J.M., B. Ozerdziejewski, H. Flohn, W.L. Hofmeyr, H.H. Lamb, K.N. Rao and C.C. Wallen, 1966: Climate Change. *WMO Technical Note*, No. 79, Geneva, WMO.
- Murakami, T., L.X. Chen and A. Xie, 1986: Relationship among seasonal cycles, low-frequency oscillations, and transient disturbances as received from outgoing longwave radiation data. *Mon. Wea. Rev.*, **114**, 1456–1465.
- Nanjundiah, R.S., 2000: Impact of moisture transport on the simulated tropical rainfall in a general circulation model. *Clim. Dyn.*, **16**, 303–317.
- and J. Srinivasan, 1999: Variations in precipitable water vapour and vertical stability during El Niño. *Geophys. Res. Lett.*, **26**, 95–97.
- , J. Srinivasan and S. Gadgil, 1992: Intraseasonal variation of the Indian summer monsoon. Part 2: Theoretical aspects. *J. Meteor. Soc. Japan*, **70**, 529–550.

- Neelin, J.D. and I.M. Held, 1987: Modeling tropical convergence based on the moist static energy budget. *Mon. Wea. Rev.*, **115**, 3–12.
- Park, C.-K., D.M. Straus and K.-M. Lau, 1990: An evaluation of the structure of tropical intraseasonal oscillations in three general circulation models. *J. Meteor. Soc. Japan*, **68**, 403–417.
- Polcher, J., 1995: Sensitivity of tropical convection to land surface processes. *J. Atmos. Sci.*, **52**, 3143–3161.
- Robock, A., C.A. Scholusser, K.Ya. Vinnikov, N.A. Spornanskaya, J.K. Entin and S. Qiu, 1998: Evaluation of AMIP soil moisture simulations. *Global and Planetary Change*, **19**, 181–208.
- Rossow, W.B. and R.A. Schiffer, 1991: ISCCP cloud data products. *Bull. Amer. Meteor. Soc.*, **72**, 2–20.
- Salby, M.L., R.R. Garcia and H.H. Hendon, 1994: Planetary-scale circulation in the presence of climatological and wave-induced heating. *J. Atmos. Sci.*, **51**, 2344–2367.
- Schemm, J., S. Shubert, J. Terray and S. Bloom, 1992: Estimates of monthly mean soil moisture for 1979–1989. *NASA Tech. Memo.*, No. 1045571, 252 pp.
- Shea, D.J., K.E. Trenberth and R.W. Reynolds, 1990: A global monthly sea surface temperature climatology. *NCAR Tech. Note, NCAR/TN-345+STR, Natl. Cent. for Atmos. Res.*, Boulder, Colorado, 167pp.
- Shen, X., M. Kimoto and A. Sumi, 1998: Role of land surface processes associated with interannual variability of broad-scale Asian summer monsoon as simulated by the CCSR/NIES AGCM. *J. Meteor. Soc. Japan*, **76**, 217–236.
- Sikka, D.R. and S. Gadgil, 1980: On the maximum cloud zone and the ITCZ over Indian longitudes during the southwest monsoon. *Mon. Wea. Rev.*, **108**, 1840–1853.
- Slingo, J.M., 1987: The development and verification of a cloud prediction scheme for the ECMWF model. *Quart. J. Roy. Meteor. Soc.*, **113**, 899–927.
- and Co-authors, 1996: Intraseasonal oscillation in 15 atmospheric general circulation models. Results from an AMIP diagnostic sub-project. *Clim. Dyn.*, **12**, 325–357.
- Spencer, R.W., 1993: Global oceanic precipitation from the MSU during 1979–1991 and comparisons to other climatologies. *J. Climate*, **6**, 1301–1326.
- Srinivasan, J., S. Gadgil and P.J. Webster, 1993: Meridional propagation of large scale monsoon convective zones. *Meteor. Atmos. Phys.*, **52**, 15–35.
- and G.L. Smith, 1996: Meridional migration of tropical convergence zones. *J. Appl. Meteor.*, **35**, 1189–1202.
- Waliser, D.E., N.E. Graham and C. Gautier, 1993: Comparison of highly reflective cloud and outgoing longwave radiation datasets for use in estimating tropical deep convection. *J. Climate*, **6**, 331–353.
- Wang, B. and H. Rui, 1990: Synoptic climatology of transient tropical intraseasonal convection anomalies: 1977–1985. *Meteor. Atmos. Phys.*, **44**, 43–62.
- Webster, P.J. and L. Chou, 1980a: Seasonal structure of a simple monsoon system. *J. Atmos. Sci.*, **37**, 354–367.
- and ———, 1980b: Low frequency transition of a simple monsoon system. *J. Atmos. Sci.*, **37**, 368–382.
- , 1983: Mechanisms of monsoon low-frequency variability: Surface hydrological effects. *J. Atmos. Sci.*, **40**, 2110–2124.
- Xie, P. and P.A. Arkin, 1997: Global precipitation: A 17-year monthly analysis based on gauge observations, satellite estimates, and numerical model outputs. *Bull. Amer. Meteor. Soc.*, **78**, 2539–2558.
- Yang, S. and K.-M. Lau, 1998: Influences of sea surface temperature and ground wetness on Asian summer monsoon. *J. Climate*, **11**, 3230–3246.
- Yasunari, T., 1979: Cloudiness fluctuations associated with the Northern Hemisphere summer monsoon. *J. Meteor. Soc. Japan*, **57**, 227–242.
- , 1981: Structure of an Indian summer monsoon system with around 40-day period. *J. Meteor. Soc. Japan*, **59**, 336–354.
- Zhang, G.J., 1994: Effect of cumulus convection on the simulated monsoon circulation in a general circulation model. *Mon. Wea. Rev.*, **122**, 2022–2038.
- Zhang, M.H., J.J. Hack, J.T. Kiehl and R.D. Cess, 1994: Diagnostic study of climate feedback processes in atmospheric general circulation models. *J. Geophys. Res.*, **99**, 5525–5537.